04,05

The effect of Bi^{3+} ion substitution on the structural-phase state and features of the magnetic structure of the $BaFe_{12-x}Bi_xO_{19}$ solid solution

© A.V. Trukhanov[1,2], S.V. Trukhanov[1,2], V.V. Korovushkin[2], V.G. Kostishin[2], V.A. Turchenko[3], T.I. Zubar[1], D. Sangaa[4], N.V. Abmetko[1], I.A. Grekov[1,5], D.B. Migas[5], D.I. Tishkevich[1]

[1] Scientific and Practical Materials Research Center, National Academy of Sciences of Belarus, Minsk, Belarus
[2] National University of Science and Technology MISiS, Moscow, Russia
[3] Joint Institute for Nuclear Research, Dubna, Russia
[4] Institute of Physics and Technology, Mongolian Academy of Sciences, Mongolia, 210651, Ulaanbaatar, Enkhtaivan av., 54B
[5] Belarusian State University of Informatics and Radioelectronics, Minsk, Belarus

E-mail: truhanov86@mail.ru

Received June 8, 2023
Revised July 11, 2023
Accepted July 12, 2023

The results of studies of the features of the phase composition, crystal and magnetic structure of Bi-substituted barium hexaferrite $BaFe_{12-x}Bi_xO_{19}$ ($0.1 \leq x \leq 1.2$) by methods of Mossbauer spectroscopy, X-ray phase analysis, as well as image analysis by scanning electron microscopy are presented. Samples of Bi-substituted hexaferrites — $BaFe_{12-x}Bi_xO_{19}$ (where $x = 0.1$; 0.3; 0.6; 0.9 and 1.2) were synthesized by the method of solid-phase reactions with double annealing (at $T = 1100°C$ for 6 h) and intermediate grinding (for 0.5 h). The X-ray phase analysis allowed us to establish the limit of substitution of Fe^{3+} ions by Bi^{3+} ions. It has been shown that at a low level of substitution ($x \leq 0.3$) there are no impurity phases detected and the samples are characterized by a single-phase state with the spatial group $P6_3/mmc$. When the degree of substitution increases ($x > 0.3$) the formation of impurity phases is noted, which can be explained by the difficulties of ion diffusion in the process of solid-phase synthesis, as well as the formation of defects in the structure of magentoplumbite due to the large ionic radius of Bi^{3+}. As impurity phases in the studied compositions ($x > 0.3$) Marked: $BiFeO_3$ (Pr. Gr. *Pnma*); BiO_2 (Pr. Gr. *Fm*-3*m*); $BaBi_2O_6$ (Pr. Gr. *R*-3) and $BaO_{0,5}Bi_{1,5}O_{2,16}$ (Pr. Gr. *Im*-3*m*). The content of the main phase (Pr. Gr. $P6_3mmc$) at the same time decreases from 95.11 to 88.27 vol.% when increasing x from 0.6 to 1.2, respectively. The analysis performed by the method of Messbaurov spectroscopy showed that all Fe ions have a charge of 3+. And all parameters lie within the values characteristic of Fe^{3+} ions corresponding to the coordination of polyhedra: 12k. 4f2, 2a — octahedra, 4f1 — tetrahedron, and 2b — bipyramide. It is possible to single out a small monotonous decrease only for the 12k position. The analysis of SEM images showed an increase in the average particle size up to 10 mkm, depending on the concentration of bismuth oxide during the synthesis of hexaferrite.

Keywords: hexaferrites, diamagnetic substitution, bismuth oxide, Mossbauer spectroscopy, X-ray phase analysis.

DOI: 10.61011/PSS.2023.08.56570.104

1. Introduction

M-type hexaferrites, with the general formula $AB_{12}O_{19}$ (where A — Ba^{2+}, Sr^{2+} or Pb^{2+}, and B — Fe^{3+} or substituent ions), have found wide application in the production of permanent magnets, interference filters, radio-absorbing coatings, devices of extremely high and ultrahigh frequencies [1–8], as well as the possibility of use in spintronics [9–13], due to its properties: non-toxicity, ease of synthesis, chemical stability, magnetic, dielectric and microwave properties [14–17]. The magnetic properties of barium hexaferrites depend both on the type of isomorphic impurity and its amount in the structure, which makes it possible not only to study their properties, but also to synthesize samples with specified characteristics for practical use.

M-type hexaferrites have a crystal structure isomorphic to the natural mineral — magnetoplumbite $PbFe_{12}O_{19}$, which was first studied by Adelskold [18]. Iron ions in the hexaferrite structure with such a structure are localized in five nonequivalent crystallographic positions: 2a, 2b, $4f_1$, $4f_2$ and 12k. Of these, 2a, $4f_2$ and 12k are octahedral, $4f_1$ — tetrahedral, and 2b forms a bipyramid. Polyhedra $4f_1$ and 2a are located in the spinel block (S), $4f_2$ and 2b in the hexagonal (R), and 12k on the border of the spinel and hexagonal blocks (RS) [19].

In unsubstituted hexaferrite $BaFe_{12}O_{19}$, a collinear magnetic structure is performed in which the magnetic moments

of positions 12k, 2a and 2b are directed in one direction, and $4f_1$ and $4f_2$ in the other, antiparallel [20], which leads to uncompensated antiferromagnetism (ferrimagnetism). The weakening of these interactions due to the substitution of Fe^{3+} ions of both groups by non-magnetic and/or weakly magnetic metal ions leads to a decrease in the resulting magnetic moment and can lead to a non-collinear magnetic structure [21]. Thus, earlier studies were conducted on the deviation from strict collinearity in the direction of magnetic moment vectors for simple and multicomponent oxides: α-Fe_2O_3 [22], γ-Fe_2O_3 [23,24], $CrFe_2O_4$ [25], CrO_2 [26], $NiFe_2O_4$, $Y_3Fe_5O_{12}$ and $Dy_2BiFe_5O_{12}$ [27]. Also, earlier studies have been conducted that demonstrated a non-collinear magnetic structure for Sc-substituted hexagonal ferrites [28]. It was shown that deviations from collinearity under conditions of chemical substitution of iron ions were most significant in the surface layer of the grain at thicknesses of several nm (which may be due to defects on the surface).

For controlled changes in magnetic and electrical properties, the principle of changing the chemical composition of hexaferrite is used. Basically, most studies are aimed at studying the substitution of Fe^{3+} ions with metal ions with a close ionic radius and an oxidation state of 3+, since the charge balance is realized quite easily (preservation of the law of electroneutrality) [29,30].

The scientific idea of the research is to determine the nature of the distribution of substituent ions with a large ionic radius (using the example of Bi^{3+} ions) in a hexagonal ferrite matrix and to establish the influence of the degree of substitution on the features of the structural-phase composition, magnetic and microwave characteristics. There are two hypotheses about the nature of the distribution of substituent ions with a large radius in the structure of hexaferrite. So, according to one hypothesis, substitution should be carried out in B-positions (by replacing ions Fe^{3+}). According to the second hypothesis, substitution should occur in A-positions (Bi^{3+} can replace a commensurate ion Ba^{2+}), which should lead to a violation of the charge balance and to a partial charge transformation Fe^{3+} into a state of Fe^{2+} to preserve electroneutrality. In this situation, the magnetic, electrical and microwave properties can be influenced by two competing factors — the influence of the energy of the crystal field and the influence of the spin state of iron ions. The substitution of ions in A-positions can lead not only to frustration of the magnetic structure, but also to the formation of a mixed valence state of iron ions (the number of Fe^{2+} ions is directly proportional to the level of concentration substitution by bismuth ions). It should be noted that in hexaferrites with a mixed valence state, anomalous effects of charge and spin ordering should theoretically be observed. Thus, for Fe^{2+} ions, a crossover of spin states can be fixed. Crossover of spin states — quantum mechanical effect. Iron ions Fe^{2+} contain six electrons on the d-shell ($3d^6$). Depending on the cleavage ratio in the local crystal field D_{cf} between t_{2g} and e_g levels and Hund energies J_h for the most common Fe^{2+} ion, two stable spin configurations. Low spin configuration (LS, $6t_{2g}$-$0e_g$, $S = 0$) and high Spin configuration (HS, $4t_{2g}2e_g$, $S = 2$). There are theoretical prerequisites for a possible intermediate state — configuration with intermediate spin (IS, $5t_{2g}$-$1e_g$, $S = 1$). Splitting in the crystal field is completely determined by the oxygen environment of iron ions in octahedral coordination and a high-spin state is realized ($S = 2$) Fe^{2+} ion, which causes distortion in the arrangement of ligands. Local distortions in the crystal structure can lead not only to a change in the parameters of the exchange interaction (when the bond lengths Fe−O and the valence angles Fe−O−Fe change), but also lead to the formation of a non-zero dipole moment (spontaneous dielectric polarization). A stable low-spin state ($S = 0$) can be realized in case of increase of D_{cf}. The possibility of implementing a state with intermediate spin ($S = 1$) is being actively discussed at present, and the corresponding calculations assume that spin-orbit interaction and quantum instability are taken into account both in t_{2g} and in e_g 3d segments- shells.

There are known works in which studies of the properties of hexaferrites with substitution by ions Bi^{3+} [31–35] were carried out. In these papers, the approaches described above are presented (when bismuth can replace both barium ions in A-positions and iron ions in B-positions. So, it was assumed in [31] that the ions Bi^{3+} replace the ions Ba^{2+}, but the authors in [32] assume that the main substitution goes by Fe^{3+}. Also the authors in [32], believe that bismuth replaces iron in exactly the positions $4f_1$ or $4f_2$, which is the reason for the increase in M_S SrM by 1.1% and 3.3% and the average grain size depending on the concentration of Bi_2O_3 in the synthesis of hexaferrites. An increase in the average grain size and a decrease in uniformity in grain size distribution, depending on the concentration of bismuth oxide during synthesis, were also noted in [33]. All synthesized SrM samples were single-phase (JCPDF #33-1340). It was also shown that at low concentrations of bismuth oxide, impurity phases of hematite were detected during the synthesis of hexaferrite. The authors attribute this phenomenon to the result of a competing reaction, which depends not only on substitution, but also on the type of organic matrix used in the synthesis of samples by the ash-gel method. A number of papers [34,35] also noted the growth of hexaferrite particles during the substitution of iron ions for bismuth ions. However, at the moment there is no clear understanding of the mechanism of substitution of large bismuth ions in the hexaferrite structure, and there is also no systematic data on the correlation of chemical composition (ion concentration Bi^{3+}), structural-phase features and magnetic structure of the solid solution $BaFe_{12-x}Bi_xO_{19}$ ($0.1 \leq x \leq 1.2$). In this regard, the purpose of this work was to study the effect of the concentration of bismuth oxide in the synthesis of M-type barium hexaferrite on the phase composition, crystal structure features, grain microstructure and magnetic structure of a solid solution of Bi-substituted M-type barium hexaferrites.

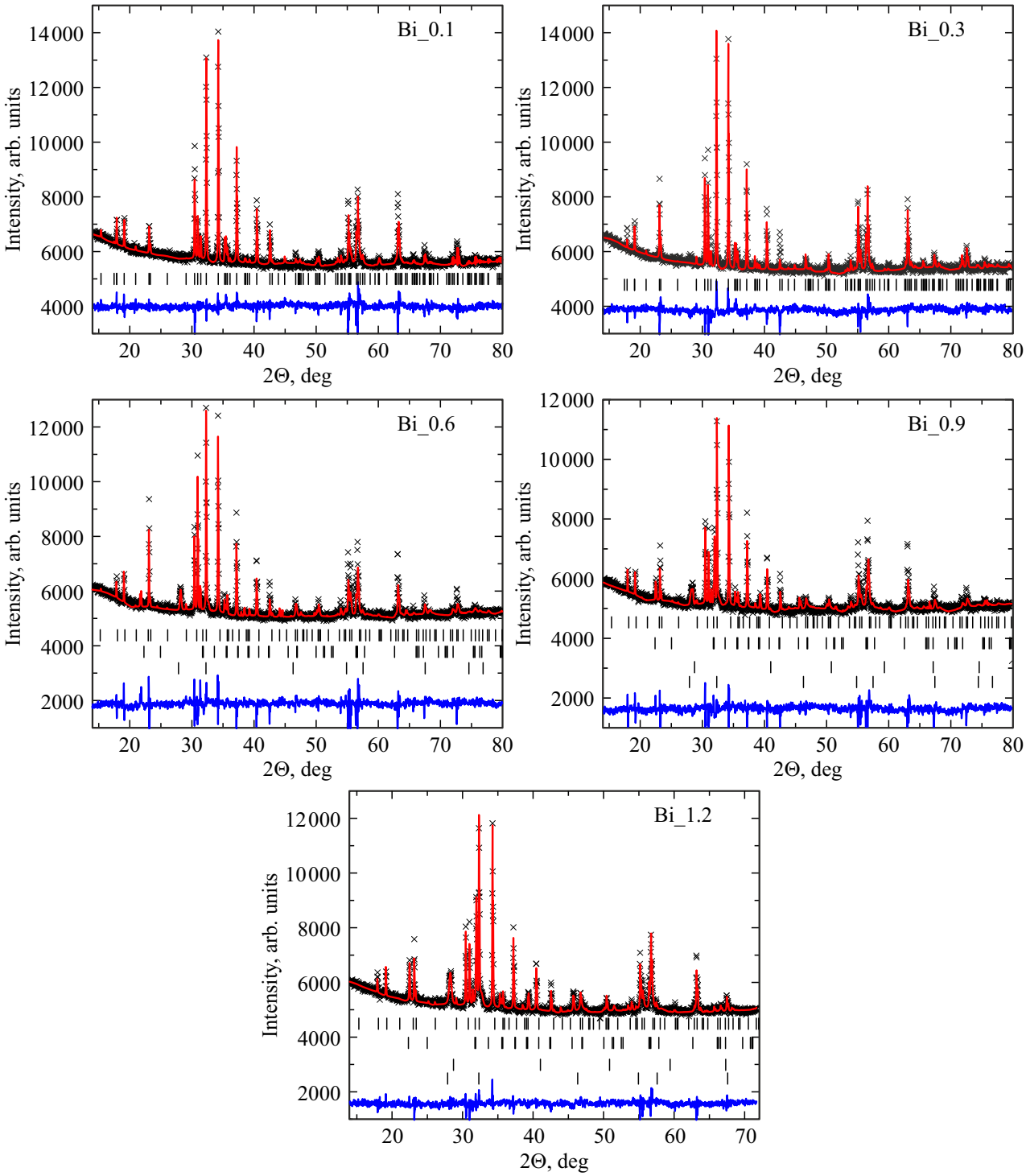

Figure 1. X-ray diffraction spectra of samples $BaFe_{12-x}Bi_xO_{19}$ ($x = 0.1-1.2$).

2. Synthesis methodology and research methods

The objects of the study are polycrystalline samples of barium hexaferrite with substitution by ions Bi^{3+} — $BaFe_{12-x}Bi_xO_{19}$ (where $x = 0.1$; 0.3; 0.6; 0.9 1.2). Samples were synthesized using ceramic technology (by solid-phase reactions) from the initial oxides of Fe_2O_3, Bi_2O_3 and BaCO carbonate$_3$ qualifications „OSH". The sample portions were calculated with an approximation that the ions Bi^{3+} should replace the ions Fe^{3+}. A mixture of oxides and carbonate taken in a strictly stoichiometric ratio was subjected to homogenization for 0.5 h in a ball mill with the addition of alcohol, then compaction and synthesizing firing in

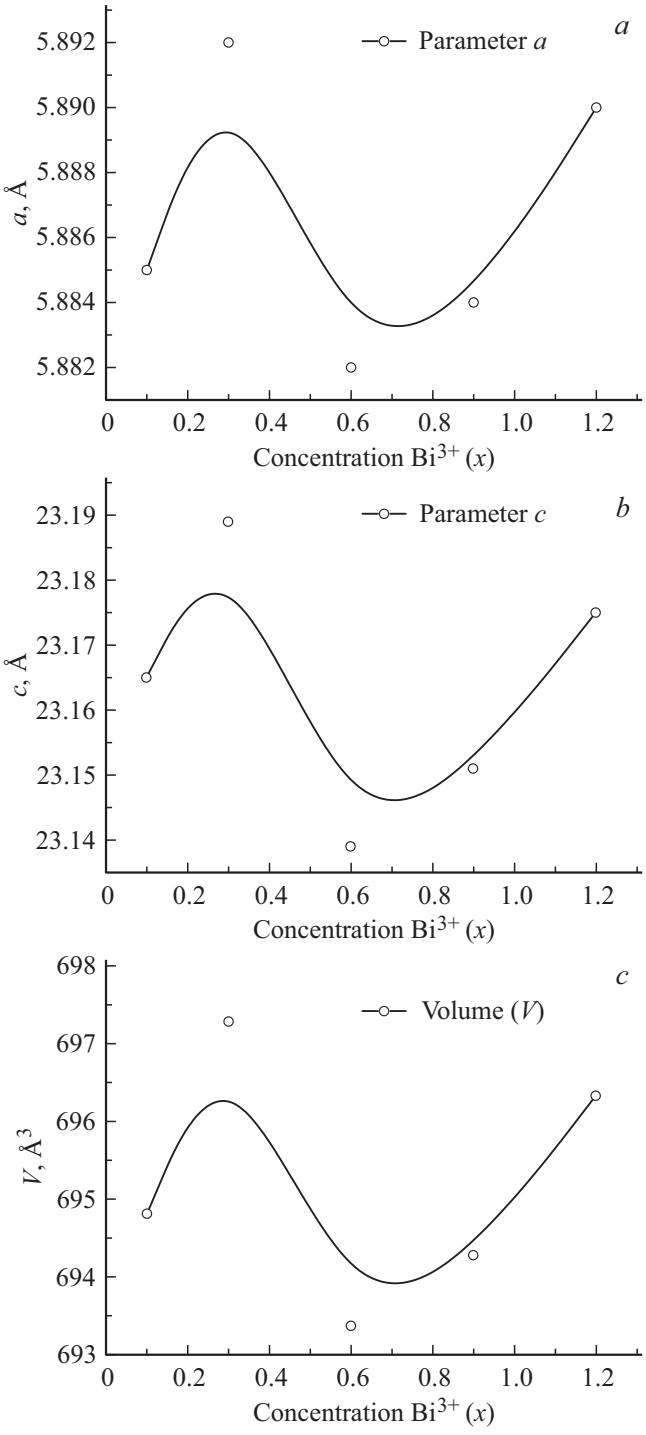

Figure 2. Concentration dependence of the parameters a (a) and c (b) of the lattice cell, as well as the volume of the lattice cell V (c) for samples $BaFe_{12-x}Bi_xO_{19}$ ($x = 0.1-1.2$).

air at 1100°C (6 h). Further, the sintered samples were mechanically crushed (in a ball mill followed by sieving through a sieve), pressed again, and then sintered again at 1100°C (6 h). After each sintering, the samples were slowly cooled in the furnace ($\sim 100°$/h) [36]. The structural-phase analysis of the research objects was performed by X-ray diffraction in Co-K_a-radiation. Point-by-point scanning mode, angle range 2θ: 20–80 degrees, step 0.03. X-ray data processing was carried out as part of a full-profile analysis using the Rietveld method [37]. The magnetic structure of the research objects was carried out by the method of Mössbauer spectroscopy on the Ms-1104 Em spectrometer at room temperature. The source of γ-radiation was Co^{57} in the rhodium matrix. The isomeric (chemical) shift was calculated relative to α-Fe. The spectra were processed using the „Univem Ms“ program, which shows the best convergence of the experimental spectrum and the decomposition model according to the parameter $\min \chi^2$ and their differences.

The microstructure of the research objects was analyzed on the basis of images obtained by scanning electron microscopy (SEM) using Carl Ziess EVO10 SEM. An equivalent diameter was measured for the particle size distribution of the study objects. The percentage of occupied area (P) was calculated using the following formula [38]:

$$P = \frac{\pi}{4}\frac{d_i^2 n_i}{S} \times 100\%,$$

where d_i — the size (diameter of the equivalent circle) of the particle, S — the total area of all particles on in the image, n_i — the number of particles of i-size.

3. Results and discussions

3.1. Phase composition and crystal structure

Figure 1 shows the X-ray diffraction spectra of the research objects. As a result of the analysis of the X-ray diffraction spectra of barium hexaferrites in the $BaFe_{12-x}Bi_xO_{19}$ system (where $x = 0.1$; 0.3; 0.6; 0.9 and 1.2), it was noted that compositions with low the concentration of bismuth ions ($x \leq 0.3$) are completely single-phase and can be described in the framework of Pr. Gr. $P6_3/mmc$ with two formula units per lattice cell ($Z = 2$). Impurity phases were noted with an increase in the concentration of bismuth ions ($x > 0.6$). So, for the composition $x = 0.6$, the content of the bulk fraction of the main phase (Pr. Gr. $P6_3/mmc$ № 194) is reduced to 95.11 vol.%. The presence of two impurity phases of the composition $BiFeO_3$ was noted (Pr. Gr. $Pnma$ № 62) — 3.45 vol.% and BiO_2 (Pr. Gr. Fm-3m № 225) — 1.44 vol.%. The content of the bulk fraction of the main phase (Pr. Gr. $P6_3/mmc$ № 194) is reduced to 93.48 vol.% for the composition $x = 0.9$. The presence of two impurity phases of the composition $BiFeO_3$ was noted (Pr. Gr. $Pnma$ № 62) — 4.65 vol.%; $BaBi_2O_6$ (Pr. Gr. R-3 № 148) — 0.4 vol.% and BiO_2 (Pr. Gr. Fm-3m № 225) — 1.41 vol.%. For the composition $x = 1.2$, the content of the bulk fraction of the main phase (Pr. Gr. $P6_3/mmc$ № 194) is reduced to 88.27 vol.%. The presence of two impurity phases of the composition $BiFeO_3$ was noted (Pr. Gr. $Pnma$ № 62) — 7.60 vol.%; $BaO_{1,5}Bi_{1,5}O_{2,16}$ (Pr. Gr. Im-3m № 229) —

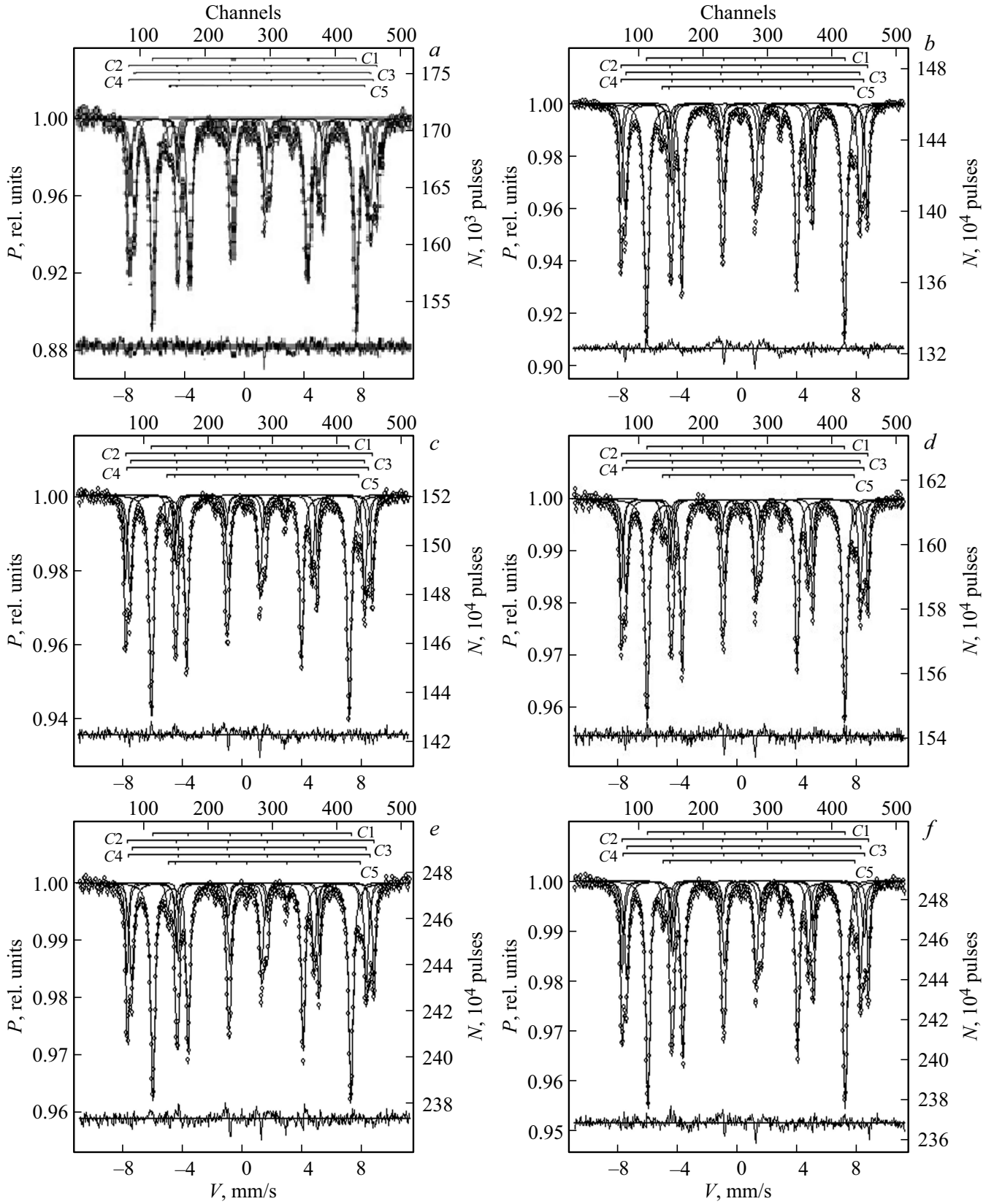

Figure 3. Mössbauer spectra of hexaferrite samples with isomorphic substitution for samples $BaFe_{12-x}Bi_xO_{19}$: *a* — 0.0, *b* — 0.1, *c* — 0.3, *d* — 0.6, *e* — 0.9, *f* — 1.2

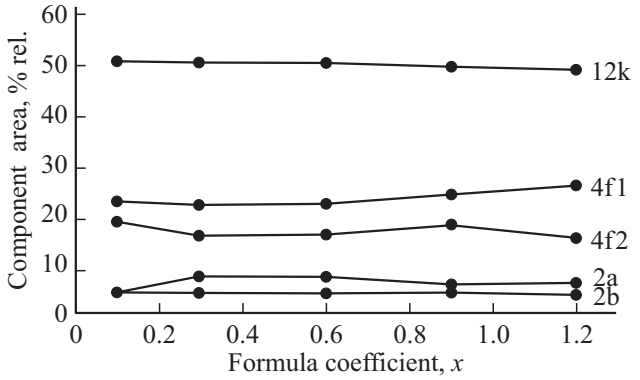

Figure 4. Dependences of the areas of the components of the spectra on the formula coefficient x for samples $BaFe_{12-x}Bi_xO_{19}$.

1.55 vol.% and BiO_2 (Pr. Gr. Fm-3m № 225) — 2.58 vol.%. Table 1 presents the results of a study of the phase composition of $BaFe_{12-x}Bi_xO_{19}$ samples (where $x = 0.1$; 0.3; 0.6; 0.9 and 1.2) performed by X-ray diffraction.

The formation of impurity phases during the synthesis of hexaferrites with a large proportion of ion substitution is a very common phenomenon. This phenomenon can be explained by the fact that the ionic radius of iron and the replacement ion are different — this leads to distortion of the crystal structure of hexaferrites and at high concentrations of the replacement impurity, a large number of distortions accumulate, which possibly allows the formation of impurity phases. In the case of substitution by bismuth ions of ion radii Fe^{3+} ($R_{Fe3+} = 0.49$ Å) for tetrahedral coordination; $R_{Fe3+} = 0.58$ Å for pentahedral coordination and $R_{Fe3+} = 0.645$ Å for octahedral coordination) [39] and Bi^{3+} ($R_{Bi3+} = 0.84$ Å for tetrahedral coordination; $R_{Bi3+} = 0.96$ Å for pentahedral coordination and $R_{Bi3+} = 1.03$ Å for octahedral coordination) [40]. The phase composition determined by X-ray diffraction data for each sample is presented in Table 2.

A nonlinear change in the structural parameters for the main phase (Pr. Gr. $P6_3/mmc$ № 194) samples $BaFe_{12-x}Bi_xO_{19}$ (where $x = 0.1$; 0.3; 0.6; 0.9 and 1.2) depending on the concentration Bi^{3+} Figure 2 shows the concentration dependence of the lattice cell parameters and the lattice cell volume of $BaFe_{12-x}Bi_xO_{19}$ samples. An increase of the lattice cell parameters from $a = 5.880$ Å and $c = 23.160$ Å was noted for $x = 0$ [11] to $a = 5.892$ Å, and $c = 23.189$ Å for $x = 0.3$ was noted at the level of small substitution concentrations ($x = 0.1$ and 0.3), where the samples are single-phase. This is due to the large ionic radius Bi^{3+} (as noted above). A sharp decrease of the parameters of the lattice cell to $a = 5.882$ Å and $c = 23.139$ Å was noted with an increase of the concentration of bismuth to $x = 0.6$, which may be caused by the deviation from the specified stoichiometry with respect to bismuth due to impurity phase formation. Further, an increase in the lattice cell parameters was noted to $a = 5.891$ Å and $c = 23.175$ Å for $x = 1.2$, which may also be due to the competition of two factors: the difference in ionic radii Fe^{3+}/Bi^{3+} and impurity phase formation processes.

3.2. Magnetic structure

Figure 3 shows the Mossbauer spectra of $BaFe_{12-x}Bi_xO_{19}$ samples. Visually, all the spectra do not differ from each other. All the spectra were decomposed into 5 sextets. Obtained parameters: isomeric shift δ (mm/s), quadrupolar splitting Δ (mm/s), magnetic field on nuclei Fe^{57} Neff (cFu), sextet areas S (% vol.), the width of the resonance lines Γ (mm/s), are given in Table 1.

It can be seen from Table 1 that iron ions correspond to the degree of oxylation 3^+ in samples of all compositions, according to the values of the isomeric shift. In this case, all parameters are within the values characteristic of the ions Fe^{3+} corresponding to the coordination of polyhedra: 12k, $4f_2$, 2a — octahedra, $4f_1$ — tetrahedron, and 2b — bipyramide [40.41]. Table 1 shows the values of the isomeric shift (δ, mm/s) for all the samples studied, as well as for unsubstituted barium hexaferrite ($x = 0$). As a result of the analysis of the Mössbauer spectroscopy data, it can be seen that the values of the isomeric shift correlate well with the values for unsubstituted barium hexaferrite. This gives reason to believe that iron ions have an oxidation state of 3+. The degree of oxidation of 2+ for iron ions is not fixed, because the values of the isomeric shift in this case would be sharply different, which is well described in the works [42,43]. It should be emphasized separately that the high-spin and low-spin states are characteristic of iron ions with an oxidation state of 2+ with a coordination number of 6 (in octahedral anionic environment). Thus, it will not be entirely correct to discuss the spin state of iron ions if the presence of iron ions with an oxidation state of 2+ is not noted in the studied samples. Absence of iron ions with a degree of oxidation 2+ may be an indirect confirmation of our assumption that the substitution of bismuth ions occurs in the B-positions.

Nevertheless, some parameters are slightly different from the theoretical ones. This concerns the areas (Fig. 4) of Fe ions ($4f_1$), which reach up to 24.63% vol. ($x = 1.2$) compared to the theoretical 16.7% rel., as well as 2b ions with an area of 4.4% rel., compared to the theoretical value of 8.3% rel. This can be explained by the higher probability of the resonant effect of tetrahedral ions Fe^{3+}, compared with octahedral ones, as explained in [44], and the lower probability of ions Fe^{3+} in the case of their localization in bipyramide, as a consequence of the greater amplitude of thermal vibrations iron ion. The areas of sextets are the most sensitive parameters to isomorphic substitutions, therefore, Fig. 4 shows their dependences on the substitution coefficient x. A small monotonic decrease can be distinguished only for the position 12k from the dependencies obtained. The remaining curves are characterized by a statistical spread of values. Assuming that a small monotonic decrease in the area from the

Table 1. Parameters of the Mössbauer spectra of samples $BaFe_{12-x}Bi_xO_{19}$

Sample	Component	Isomeric shift δ, mm/s	Quadrupole splitting, Δ mm/s	Magnetic fields H_{eff}, kOe	Area component S, %	Width lines Γ, mm/s	Interference
$x = 0$	$C1(Fe^{3+})_{VI}$	0.35	0.42	414	50.5	0.32	12k
	$C2(Fe^{3+})_{VI}$	0.38	0.20	516	16.8	0.29	$4f_2$
	$C3(Fe^{3+})_{IV}$	0.26	0.22	489	19.8	0.31	$4f_1$
	$C4(Fe^{3+})_{VI}$	0.34	0.01	507	7.5	0.26	2a
	$C5(Fe^{3+})_{V}$	0.28	2.21	400	5.4	0.30	2b
$x = 0.1$	$C1(Fe^{3+})_{VI}$	0.36	0.42	415	50.3	0.35	12k
	$C2(Fe^{3+})_{VI}$	0.39	0.19	516	17.5	0.28	$4f_2$
	$C3(Fe^{3+})_{IV}$	0.27	0.21	491	21.9	0.33	$4f_1$
	$C4(Fe^{3+})_{VI}$	0.34	0.01	507	5.4	0.21	2a
	$C5(Fe^{3+})_{V}$	0.28	2.21	402	4.9	0.27	2b
$x = 0.3$	$C1(Fe^{3+})_{VI}$	0.36	0.42	414	49.9	0.33	12k
	$C2(Fe^{3+})_{VI}$	0.38	0.21	516	14.3	0.28	$4f_2$
	$C3(Fe^{3+})_{IV}$	0.27	0.27	491	20.7	0.31	$4f_1$
	$C4(Fe^{3+})_{VI}$	0.36	0.04	507	10.3	0.30	2a
	$C5(Fe^{3+})_{V}$	0.29	2.22	400	4.8	0.24	2b
$x = 0.6$	$C1(Fe^{3+})_{VI}$	0.36	0.42	415	49.8	0.34	12k
	$C2(Fe^{3+})_{VI}$	0.38	0.20	518	14.6	0.23	$4f_2$
	$C3(Fe^{3+})_{IV}$	0.27	0.21	492	20.7	0.32	$4f_1$
	$C4(Fe^{3+})_{VI}$	0.37	0.04	506	9.7	0.31	2a
	$C5(Fe^{3+})_{V}$	0.29	2.21	402	5.2	0.29	2b
$x = 0.9$	$C1(Fe^{3+})_{VI}$	0.35	0.42	415	49.1	0.33	12k
	$C2(Fe^{3+})_{VI}$	0.39	0.21	516	16.8	0.27	4f2
	$C3(Fe^{3+})_{IV}$	0.27	0.20	492	23.1	0.35	$4f_1$
	$C4(Fe^{3+})_{VI}$	0.33	−0.02	509	6.3	0.22	2a
	$C5(Fe^{3+})_{V}$	0.28	2.2	401	4.7	0.24	2b
$x = 1.2$	$C1(Fe^{3+})_{VI}$	0.35	0.41	413	48.8	0.35	12k
	$C2(Fe^{3+})_{VI}$	0.39	0.22	515	14.1	0.24	$4f_2$
	$C3(Fe^{3+})_{IV}$	0.28	0.19	491	24.6	0.36	$4f_1$
	$C4(Fe^{3+})_{VI}$	0.34	−0.03	509	8.0	0.28	2a
	$C5(Fe^{3+})_{V}$	0.27	2.24	400	4.5	0.23	2b

Table 2. Phase composition of samples $BaFe_{12-x}Bi_xO_{19}$ obtained from the analysis of X-ray diffraction spectra

Concentration $Bi^{3+}(x)$	Content basic phases $BaFe_{12}O_{19}$ $P6_3/mmc$, vol.%	Content impurity Phases $BiFeO_3$ $Pnma$, vol.%	Content impurity Phases BiO_2 Fm-3m, vol.%	Content impurity phases $BaBi_2O_6$ R-3, vol.%	Content impurity phases $BaO_{0.5}Bi_{1.5}O_{2.16}$ Im-3m, vol.%
0.1	100	–	–	–	–
0.3	100	–	–	–	–
0.6	95.11	3.45	1.44	–	–
0.9	93.48	4.65	1.41	0.46	–
1.2	88.27	7.60	2.58	–	1.55

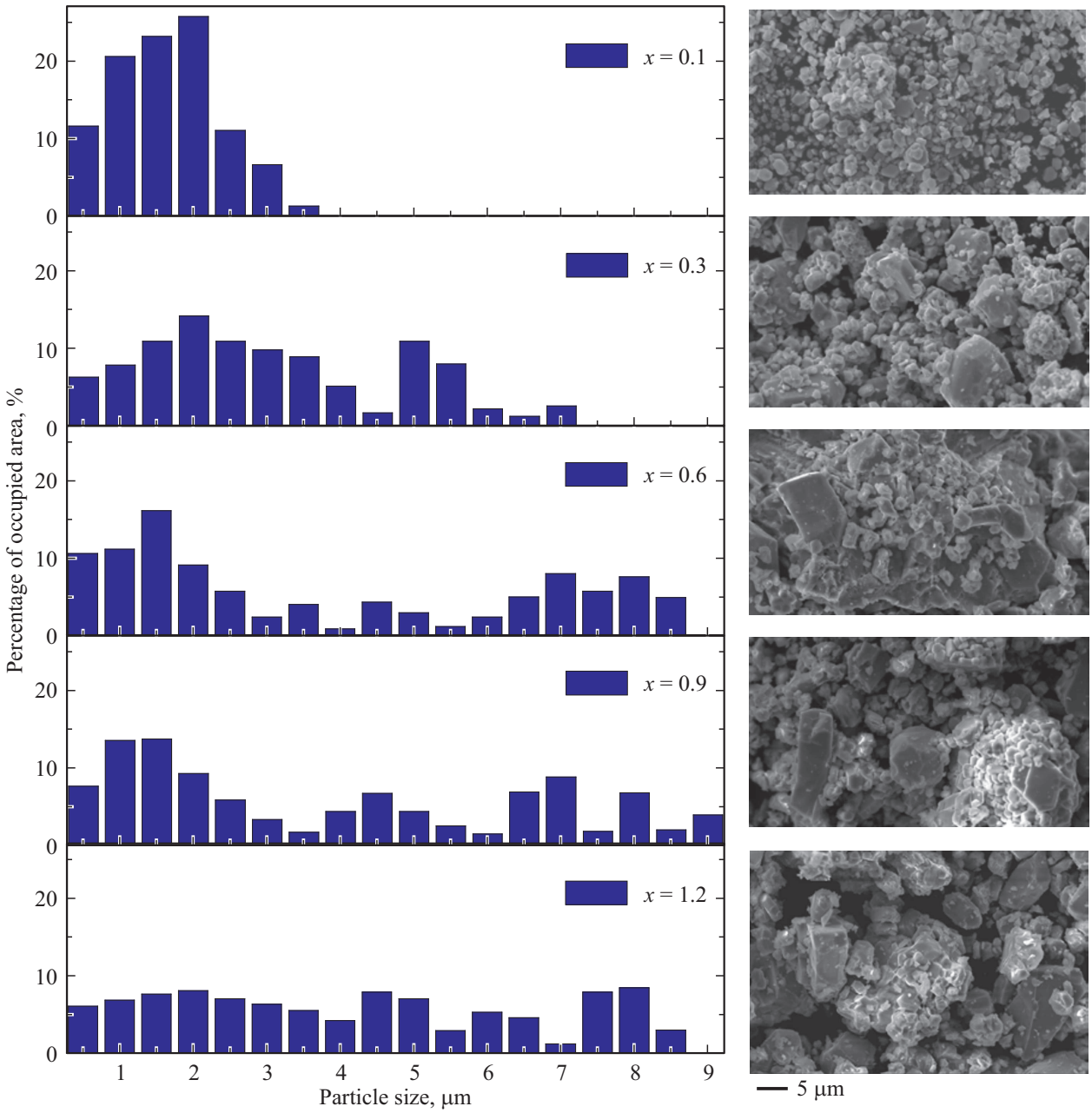

Figure 5. Particle size distribution of samples $BaFe_{12-x}Bi_xO_{19}$ (left column) and corresponding SEM images with magnification x5000 (right column).

ions Fe^{3+} of the position 12*k* is associated with the occurrence of Bi ions, then at $x = 1.2$ it will be 1.75% rel., and when converted to the formula coefficient x will be equal to 0.3. Considering that the ionic radius Bi^{3+} (coord. number VI) is 1.17 Å, and Fe^{3+} (coordination number VI) 0.67 Å, ion substitution Fe ions Bi at the degree of substitution $x > 0.3$ is unlikely. Therefore, 2 variants are possible at higher concentrations: ions Bi^{3+} replaces ions Ba^{2+}, or bismuth remains in the form of Bi_2O_3 and no isomorphic substitutions occur. Then the ions adjacent to the vacancies should have increased local distortions of polyhedra, however if substitution occurs according to the scheme $3Ba^{2+}$ by $2Fe^{3+}$, this is not observed by the values of quadrupolar splittings. Therefore, the radiography data should record Bi_2O_3 and an increase in its content as x increases.

3.3. Investigation of microstructural parameters

Figure 5 shows the distribution of the average particle size and SEM images for the samples under study. It is possible to distinguish clear grains of regular hexagonal shape (especially for samples with small degrees of substitution) in the SEM images for $BaFe_{12-x}Bi_xO_{19}$. An agglomeration

of particles with an increase in grain size was noted with an increase of the degree of substitution by bismuth ions. This may be a consequence of glass transition processes due to the fusibility of bismuth oxide. The analysis of hexaferrite surface images and the construction of a histogram of particle size distribution based on them (Fig. 5) showed that the sample $BaFe_{12-x}Bi_xO_{19}$, with a degree of substitution $x = 0.1$ is characterized by unimodal the particle size distribution with an average size of about 1.5−2.0 and is not replaced by large particles.

An increase in the degree of substitution to $x = 0.3$ leads to the formation of grains with sizes up to $7\,\mu$m, while the largest number of grains have an area of $2\,\mu$m — 5 c. A further increase of the concentration of bismuth oxide during the synthesis of barium hexaferrite to $x = 0.6$ causes active agglomeration of small grains on the surface of large ones, whose sizes reach up to $9\,\mu$m, as can be seen in the distribution. An increase of the degree of substitution and heterogeneity of samples is the reason for the presence of a large number of unsaturated bonds in ferrite particles, which often contributes to their agglomeration. An increase of the degree of substitution to $x = 0.9$ and $x = 1.2$ does not cause significant changes in the grain size structure and distribution. It is possible only to note the intensification of particle agglomeration processes and a statistically more uniform distribution of their sizes in the range from about 0.3−0.5 to 9.0−10.0 μm. The increase of the degree of substitution and heterogeneity, as well as the grain size of the samples is due to the following factors: 1) an increase of the distortion of the crystal lattice of hexaferrite, when the ions Fe^{3+} are substituted by Bi^{3+}. 2) transport properties of bismuth oxide, as you can see, grain growth goes up to a certain point $x = 0.6$, a further increase in the proportion of substitution does not carry significant changes in size.

4. Conclusion

A solid solution of Bi-substituted hexaferrites $BaFe_{12-x}Bi_xO_{19}$ was synthesized by the method of solid-phase reactions (where $x = 0.1$; 0.3; 0.6; 0.9 and 1.2). Studies of the structural-phase state of the samples were carried out $BaFe_{12-x}Bi_xO_{19}$ (where $x = 0.1$; 0.3; 0.6; 0.9 and 1.2) by X-ray diffraction in Co-K_a radiation. It was found that samples with a low degree of substitution ($x \leq 0.3$) are single-phase and can be described in the framework of Pr. Gr. $P6_3/mmc$ № 194. An increase of the lattice cell parameters of these compositions was shown, which correlates well with the values of the ion radii Fe^{3+}/Bi^{3+}. Impurity phase formation of $BaFe_{12-x}Bi_xO_{19}$ samples (where $x > 0.6$) was noted, which can be explained by difficulties in the diffusion of ions (iron, bismuth and barium) during solid-phase synthesis, and also, the formation of defects in the structure of magentoplumbite due to the large ionic radius Bi^{3+}. A sharp decrease of the parameters of the lattice cell was noted with an increase in the concentration of bismuth to 0.6, which may be the result of a deviation from the set stoichiometry for bismuth due to impurity phase formation. Further, an increase in the parameters of the lattice cell is shown with an increase in the concentration of bismuth from $x = 0.6$ to $x = 1.2$ which may be attributable to the competition of two factors: the difference in ionic radii Fe^{3+}/Bi^{3+} and processes of impurity phase formation.

Samples of $BaFe_{12-x}Bi_xO_{19}$ were studied using Mössbauer spectroscopy method. The results indicate that iron ions correspond to a valence of 3+ in samples of all compositions, according to the values of the isomeric shift. In this case, all parameters are within the values characteristic of the ions Fe^{3+} corresponding to the coordination of polyhedra: 12k. 4f2, 2a — octahedra, 4f1 — tetrahedron, and 2b — bipyramide. It is possible to single out a small monotonic decrease only for the position 12k. Assuming that a small monotonic decrease of the area from the ions of the Fe^{3+} position 12k is associated with the occurrence of Bi ions, then at $x = 1.2$ this will be 1.75% rel., and when converted to a formula coefficient x will be equal to 0.3. A possible substitution scheme is provided at concentrations $x > 0.3$.

Scanning electron microscopy studies and image analysis were performed to determine the effect of concentration substitution with Bi^{3+} ions on the microstructure parameters of $BaFe_{12-x}Bi_xO_{19}$ samples. It was shown that samples with $x > 0.3$ have regions with heterogeneous composition. It was found that samples with a low degree of substitution ($x = 0.1$) are characterized by a unimodal distribution of particle sizes with an average value of 1.5−2.0 μm. An increase of the concentration of bismuth ($x = 0.3$ and 0.6) causes an active agglomeration of particles with sizes up to 9−10 μm and the bimodal nature of the particle size distribution is noted in the samples. A further increase of the concentration of bismuth ($x = 0.9$−1.2) is marked by an asymmetric distribution with a particle size up to 10 μm.

Funding

The studies were supported by a joint Belarusian-Mongolian project of the Belarusian Republican Foundation for Basic Research (project F22Mn-006 in Belarus and project Shu_B_2022/6 in Mongolia).

Conflict of interest

The authors declare that they have no conflict of interest.

References

[1] S.B. Narang, K. Pubby. J. Magn. Magn. Mater. **519**, 167163 (2020). DOI: 10.1016/j.jmmm.2020.167163.
[2] P. Thakur, D. Chahar, S. Taneja, N. Bhalla, A. Thakur. Ceram. Int. **46**, *10*, 15740 (2020). DOI: 10.1016/j.ceramnit.2020.03. 287.
[3] A. Houbi, A.A. Zharmenov, Y. Atassi, Z.T. Bagasharova, S. Mirzalieva, K. Kadyrakunov. J. Magn. Magn. Mater. **529**, 167839 (2021). DOI: 10.1016/j.jmmm.2021.167839.

[4] G. Srinivasan, I.V. Zavislyak, M. Popov, G. Sreenivasulu, Y.K. Fetisov. J. Jpn Soc. Powder Powder Met. **61**, S25 (2014). DOI: 10.2497/jspm.61.s25.
[5] C. de Julián Fernández, C. Sangregorio, J. de la Figuera, B. Belec, D. Makovec, D. Quesada. J. Phys. D **54**, *15*, 153001 (2021). DOI: 10.1088/1361-6463/abd272.
[6] A. Talaat, M.V. Suraj, K. Byerly, A. Wang, Y. Wang, J.K. Leea, P.R. Ohodnicki. J. Alloys Compd. **870**, 159500 (2021). DOI: 10.1016/j.jallcom. 2021.159500.
[7] E.J.J. Mallmann, A.S.B. Sombra, J.C. Goes, P.B.A. Fechine. Solid State Phenom. **202**, 65 (2013). DOI: 10.4028/www.scientific.net/ssp.202.65.
[8] M. Chandel, V.P. Singh, R. Jasrotia, K. Singha, R. Kumar. AIMS Mater. Sci. **7**, *3*, 244 (2020). DOI: 10.3934/matersci.2020.3.244.
[9] A.V. Trukhanov, V.O. Turchenko, I.A. Bobrikov, S.V. Trukhanov, I.S. Kazakevich, A.M. Balagurov. J. Magn. Magn. Mater. **253**, 393 (2015).
[10] Y. Tokunaga, Y. Kaneko, D. Okuyama, S. Ishiwata, T. Arima, S. Wakimoto, K. Kakurai, Y. Taguchi, Y. Tokura. Phys. Rev. Lett. **105**, 257201-4 (2010).
[11] A.V. Trukhanov, V.A. Turchenko, V.G. Kostishin, F. Damay, F. Porcher, N. Lupu, B. Bozzo, I. Fina, S. Polosan, M.V. Silibin, M.M. Salem, D.I. Tishkevich, S.V. Trukhanov. J. Alloys Compd. **886**, 161249 (2021).
[12] D.A. Vinnik, V.V. Kokovkin, V.V. Volchek, V.E. Zhivulin, P.A. Abramov, N.A. Cherkasova, Zhipeng Sun, M.I. Sayyed, D.I. Tishkevich, A.V. Trukhanov. Mater. Chem. Phys. **270**, 124818 (2021).
[13] G. Tan, X. Chen. J. Magn. Magn. Mater. **327**, 87 (2013).
[14] A.V. Trukhanov, S.V. Trukhanov, L.V. Panina, V.G. Kostishyn, D.N. Chitanov, I.S. Kazakevich, An.V. Trukhanov, V.A. Turchenko, M. Salem. Ceram. Int. **3**, 5635 (2017).
[15] V.E. Zhivulin, D.P. Sherstyuk, O.V. Zaitseva, N.A. Cherkasova, D.A. Vinnik, S.V. Taskaev, E.A. Trofimov, S.V. Trukhanov, S.I. Latushka, D.I. Tishkevich, T.I. Zubar, A.V. Trukhanov. Nanomater. **12**, 1306 (2022).
[16] V.E. Zhivulin, E.A. Trofimov, O.V. Zaitseva, D.P. Sherstyuk, N.A. Cherkasova, S.V. Taskaev, D.A. Vinnik, Yu.A. Alekhina, N.S. Perov, D.I. Tishkevich, T.I. Zubar, A.V. Trukhanov, S.V. Trukhanov. Cer. Int. **49**, *1*, 1069 (2023).
[17] P.V. Boikachev, A.S. Solonar, V.O. Isaev, I.A. Dubovik, A.A. Sut'ko, T.I. Zubar', D.I. Tishkevich. J. Eng. Phys. Thermophys. **95**, 5 (2022).
[18] V. Adelskold. Arkiv för mineralogi och geologi A **12**, 1 (1938).
[19] R.C. Pullar. Prog. Mater. Sci. **57**, 1191 (2012).
[20] I. Smith, H. Vane. Ferrites. IL, M. (1962), 504 p. (in Russian).
[21] V.V. Korovushkin, M.N. Shipko, V.G. Kostishin, I.M. Isayev, A.Yu. Mironovich, S.V. Trukhanov, A.V. Trukhanov. Neorgan. materialy **55**, *10*, 1065 (2019) (in Russian).
[22] A.M. der Kraan. Phys. Status Solidi **18**, 215 (1973).
[23] A.H. Morrish, K. Haneda, P.J. Schurer, J. de Physique, Colloque C6 37, C6-301. (1976).
[24] P.M.A. De Bakker, E. De Grave, R.E. Vandenberghe, L.H. Bowen. Hyperfine Interact. **54**, 493 (1990).
[25] A. Berkowitz, J. Lahut, C. VanBuren, IEEE Trans. Magn. **16**, 184 (1980).
[26] K. Haneda, H. Kojima, A.H. Morrish, P.J. Picone, K. Wakai. J. Appl. Phys. **53**, 2686 (1982).
[27] A.H. Morrish, K. Haneda, X.Z. Zhou. Nanophase Mater. Synth. 515 (1994).
[28] A.S. Kamzin, L.P. Olkhovik, V.L. Rosenbaum. FTT **41** 483 (1999). (in Russian).
[29] A.S. Kamzin, L.P. Olkhovik. FTT **41**, *10*, 1806 (1999). (in Russian).
[30] V.V. Korovushkin, A.V. Trukhanov, M.N. Shipko, V.G. Kostishin, I.M. Isayev, A.Yu. Mironovich, S.V. Trukhanov. Zhurn. neorgan. khimii **64**, *5*, 463 (2019). in Russian).
[31] H. Basma, H.T. Rahal, R. Awad. J. Magn. Magn. Mater. **539**, 168413 (2021).
[32] E.S. Lim, K.R. Mun, Y.M. Kang. J. Magn. Magn. Mater. **464**, 26 (2018).
[33] Y. Dai, Z. Lan, Z. Yu, K. Sun, X. Zhang, X. Jiang, C. Wu, W. Tong. J. Magn. Magn. Mater. **540**, 168443 (2021).
[34] K. Chokprasombat, A. Lohmaah, S. Pinitsoontorn, Ch. Sirisathitkul. J King Saud Univ Sci. **34**, *1*, 101682 (2022).
[35] S. Güner, I.A. Auwal, A. Baykal, H. Sözeri. J. Magn. Magn. Mater. **416**, 261 (2016).
[36] I. Auwal, A. Baykal, S. Güner, H. Sözeri. Ceram. Int. **43**, *1*, 1298 (2017).
[37] A.V. Trukhanov, K.A. Darwish, M.M. Salem, O.M. Hemeda, M.I. Abdel Ati, M.A. Darwish, E.Y. Kaniukov, S.V. Podgornaya, V.A. Turchenko, D.I. Tishkevich, T.I. Zubar, K.A. Astapovich, V.G. Kostishyn, S.V. Trukhanov. J. Alloys Compd. **866**, 158961 (2021).
[38] D. Tishkevich, S. Grabchikov, T. Zubar, D. Vasin, S. Trukhanov, A. Vorobjova, D. Yakimchuk, A. Kozlovskiy, M. Zdorovets, S. Giniyatova, D. Shimanovich, D. Lyakhov, D. Michels, M. Dong, S. Gudkova, A. Trukhanov. Nanomater. **10**, 1245 (2020).
[39] R.C. Pullar. Prog. Mater. Sci. **57**, 1191 (2012).
[40] http://abulafia.mt.ic.ac.uk/shannon/radius.php?Element=Fe
[41] http://abulafia.mt.ic.ac.uk/shannon/radius.php?Element=Bi
[42] V.G. Kostishin, V.V. Korovushkin, I.M. Isayev, A.Yu. Mironovich, S.V. Trukhanov, V.A. Turchenko, K.A. Astapovich, A.V. Trukhanov. FTT **63**, 229 (2021) (in Russian).
[43] V.G. Kostishin, V.V. Korovushkin, K.V. Poholok, A.V. Trukhanov. FTT **10**, 1496 (2021). (in Russian).
[44] S.V. Trukhanov, A.V. Trukhanov, V.A. Turchenko, An.V. Trukhanov, E.L. Trukhanova, D.I. Tishkevich, V.M. Ivanov, T.I. Zubar, M. Salem, V.G. Kostishyn, L.V. Panina, D.A. Vinnik, S.V. Gudkova. Ceram. Int. **44**, *1*, 290 (2018).

Translated by A.Akhtyamov